NACA

RESEARCH MEMORANDUM

HEAT TRANSFER AND PRESSURE MEASUREMENT ON A 5-INCH HEMISPHERICAL CONCAVE NOSE AT A MACH NUMBER OF 2.0

By J. Thomas Markley

Langley Aeronautical Laboratory
Langley Field, Va.

NATIONAL ADVISORY COMMITTEE
FOR AERONAUTICS

WASHINGTON
July 17, 1958

Unclassified

NASA Tech Rib Announcement #74

(CHANGE)

By 3 Mar 61

NK

(GRADE OF OFFICER MAKING CHANGE)

23 Feb 61

DATE

K

NATIONAL ADVISORY COMMITTEE FOR AERONAUTICS

RESEARCH MEMORANDUM

HEAT TRANSFER AND PRESSURE MEASUREMENT ON A 5-INCH HEMISPHERICAL CONCAVE NOSE AT A MACH NUMBER OF 2.0*

By J. Thomas Markley

SUMMARY

A 5-inch-diameter hemispherical concave nose was tested at a Mach number of 2.0 in a free jet to determine heat transfer and pressure distribution. The tests were made under sea-level conditions for a Reynolds number per foot of about 14×10^6.

The concave-nose stagnation-point heating is 40 percent of that of a hemisphere nose shape having the same diameter. At angles of attack of $\pm 5^\circ$ and $\pm 10^\circ$ there is no increase in the heat-transfer coefficient of the nose. However, some increase in heat-transfer coefficient is shown for the afterbody section of the model for windward angles of attack. Pressures measured up to 60° on the concave part of the model were equal to total pressure behind the shock at all angles of attack.

INTRODUCTION

The Langley Pilotless Aircraft Research Division is currently investigating blunt nose shapes for application to the design of supersonic missiles. Blunt nose shapes have considerably less heat transfer than a pointed nose tip. The hemisphere and flat-face nose shapes have been tested extensively. It has been shown that the stagnation-point heat transfer to a flat face is one-half, or less, that to the stagnation point of a hemisphere. Several investigators have suggested that a concave nose shape would probably have even less stagnation-point heating than the flat face. Reference 1 presented heat-transfer coefficients for several blunt shapes with modest depressions at the nose; however, no beneficial effects of these depressions were noted. Other tests of concave nose shapes like those reported in reference 2, which includes tests directed toward the study of heating in concave hemispherical depressions, have indicated stagnation heating rates considerably less

*Title, Unclassified.

than for the hemisphere. In order to evaluate the heat-transfer coefficient of a concave nose shape in more detail, at the lip and at angle of attack as well as at the stagnation point, a concave nose has been tested and the results are reported herein.

SYMBOLS

α	angle of attack, deg
c_w	specific heat of skin, Btu/lb-$^\circ$F
ρ_w	mass density of skin, lb/cu ft
h	local aerodynamic heat-transfer coefficient, Btu/(sec)(sq ft)($^\circ$F)
h_s	$\frac{h}{h_{stag\ of\ hemisphere}}$
h_{stag}	stagnation point heat-transfer coefficient, Btu/(sec)(sq ft)($^\circ$F)
M	Mach number
N_{Pr}	Prandtl number
p_t	total pressure ahead of shock, lb/sq ft
p_l	local static pressure, lb/sq ft
p_∞	free-stream static pressure, lb/sq ft
$p_{t,2}$	total pressure behind normal shock, lb/sq ft
S	distance along surface from center line, in.

S_l maximum distance along surface from center line to lip, in.

t_w skin thickness, ft

T_{aw} adiabatic wall temperature, $^{\circ}R$

T_t free-stream stagnation temperature, $^{\circ}R$

T_w wall temperature, $^{\circ}R$

T static temperature ahead of shock, $^{\circ}R$

η_r recovery factor

θ angle between the model surface and the free-stream direction, deg

τ time, sec

T_l local temperature behind normal shock

φ angle from vertical reference plane, deg

APPARATUS AND TESTING

All tests were conducted at the preflight jet of the Langley Pilotless Aircraft Research Station at Wallops Island, Va. This blowdown jet has true sea-level conditions.

The model was located with its center line on the center line of the jet with its face 2 inches downstream of the nozzle. Figure 1 shows the model before it was swung into the jet stream. The model was moved downstream so that the picture could be taken. The model was within the Mach diamond. Shadowgraph pictures were made during all tests and are shown in figures 2 to 4 for angles of attack of 0°, 5°, and 10°. From these figures no interaction with the Mach diamond of the jet can be seen.

The pressures were measured by using Statham gages which are accurate to within ±1 percent. The temperatures are measured by thermocouples which have the junction box at the base of the stand. The reference junction temperature is measured by reading a thermometer located in a box which is free of any wind currents.

MODEL

The dimensions of the model are shown in figure 5. The model was made of Inconel, of a nominal 0.050-inch thickness, but because of the spinning process used in the construction, the thickness of the skin varied. These variations are tabulated in figure 5. No support was given the skin other than the model shape itself.

Instrumentation consisted of chromel-alumel thermocouples (No. 30 gage) welded to the interior of the skin. A ray of thermocouples and pressure orifices were located 180° from each other so that when the thermocouples were windward for a test at angle of attack, the pressure orifices were leeward by the same angle. There were 15 thermocouples and 11 pressure orifices located at positions shown in figure 5. The inside diameter of the pressure orifices was 0.050 and the tubing length to the Statham gages was 5 feet.

The surface roughness of the model was about 15 microinches as measured by a Physicists Research Co. Profilometer, Model No. 11, Type 9, for the initial tests; however, during the ensuing runs the roughness increased from 15 to an estimated value of 30 microinches.

TEST CONDITIONS

The model was tested at a Mach number of 2.0 at angles of attack of 0°, ±5°, and ±10°. All tests were made in a free jet with a 27- by 27-inch nozzle which allowed testing at constant sea-level pressure and temperature for 8 seconds. Reynolds number of the test based on body diameter was 6.4×10^6. The model was injected into the airstream and was on center line approximately 0.1 second after steady-flow conditions of the jet had been reached.

DATA REDUCTION

The aerodynamic heat-transfer coefficients were calculated from data measured during the transient heating of the model at the earliest possible time, which was 0.1 second after the model was on center line. At this time the estimated radiative and conductive heat loss to the

air behind the model was negligible. The heat-transfer coefficients were calculated by using the equation

$$h = \frac{\rho_w c_w t_w}{T_{aw} - T_w} \frac{dT_w}{d\tau}$$

The time rate of change of wall temperature was obtained from plots of the wall temperature as a function of time. The heat-transfer coefficient was then evaluated by using a mass density for Inconel of 518 lb/cu ft and a specific heat of 0.11 as given in reference 3. Measured values of skin thickness were used in all calculations.

In the case where the thermocouple was located internally on the lip, the following equation was used to take in the variations in surface area:

$$h = \frac{\rho_w c_w t_w \left(\frac{1 + \frac{R_1}{R_2}}{2}\right) \frac{dT}{d\tau}}{T_{aw} - T_w}$$

where R_1 is the inside radius of the lip and R_2 is the outside radius. This expression gives an effective thickness of the Inconel; as the result of the equation, the average thickness is obtained by dividing the volume of the material by the surface area. The value for the effective thickness was 75 percent of the actual measured thickness.

The adiabatic wall temperature was obtained by using the equation

$$T_{aw} = T_t \left[\eta_r \left(1 - \frac{T_l}{T_t}\right) + \frac{T_l}{T_t}\right]$$

where $\eta_r = \left(N_{Pr}\right)^{1/2}$. The fact that $\left(N_{Pr}\right)^{1/2}$ varies over the temperature range makes little difference since the minimum ratio of $\frac{T_l}{T_t}$ on the body was 0.9. The equation used to calculate the heating rates assumes constant temperature through the wall.

RESULTS AND DISCUSSION

Pressure Distribution

Figures 6 and 7 show the pressure distribution for the model at angles of attack of 0°, ±5°, and ±10°. The local measured pressure was divided by the maximum measured pressure to obtain the ratio of local pressure to total pressure behind the shock as presented in figures 6 and 7. Figure 6 shows the windward pressure distribution plotted against the distance along the surface from the stagnation point. For all angles of attack, the three pressure stations up to and including the 60° station, which was the last station at which measurements were taken on the concave part, measured total pressure behind the shock. The dotted line represents a fairing of the data for the 0° angle-of-attack test. The five pressure-measuring orifices on the lip recorded free-stream static pressures for the 0° angle-of-attack test. All pressure gages on the lip were of low range ±15 lb/sq in.

Figure 7 represents leeward pressure distribution plotted against surface distance from the stagnation point. As in figure 5, the dotted line represents a fairing of the data for the 0° angle-of-attack test. The leeward tests also show total pressure behind the shock for the three measuring stations up to 60° on the concave part. Figures 6 and 7 show that for these test conditions the model experienced total pressure behind the shock up to and including the 60° station which was the last station at which measurements were taken between 60° and the lip.

Heat Transfer

Figure 8 shows the wall-temperature distribution for the model at angles of attack of 0°, ±5°, and ±10°. The faired line indicated by 0 seconds represents the wall temperature at which time the heat-transfer coefficients were obtained as represented in figures 9 and 10.

Figures 9 and 10 show the heat-transfer distribution for the model at angles of attack of 0°, ±5°, and ±10°. Figure 9 presents the heat transfer for the windward test at 5° and 10°. The dotted line is the fairing for the data at an angle of attack of 0°. This figure shows that out to the station where S = 3.25 inches (75°) the heat transfer remains fairly constant. The station immediately inside the lip (T_7) experienced the highest heat transfer, but it is important to note that this heat transfer remains constant with windward angle of attack. The lip at a windward angle of 10° experienced heat-transfer coefficients only 22 percent higher than those at an angle of attack of 0°. The lowest heat-transfer coefficients are on the cylinder which is in a region of low

pressure. The heat-transfer coefficients on the cylinder are the highest when the model is at windward angles of attack of 5° and 10°. The maximum heat-transfer coefficient for the test at an angle of attack of 5° is 21 percent higher than that for the test at 0°, and the maximum for the test at 10° is 31 percent higher.

Figure 10 presents the heat-transfer coefficients for the leeward test at 5° and 10°. The dotted line connects the points from the test at an angle of attack of 0°. This figure shows that the heat-transfer coefficients for the leeward test, up to station S = 3.25 inches (75°) are the same as for the windward test. The highest heat-transfer coefficient experienced in the leeward tests is on the inside of the lip (T_7), the same as in the windward tests. On the cylinder of the model the heat transfer is lower than that of the 0° angle-of-attack test. The lip, at a leeward angle of attack of 10°, experienced 30 percent lower heat-transfer coefficients than those of the 0° angle-of-attack test.

In figure 11, heating rates obtained for the model at an angle of attack of 0° are compared with those obtained experimentally and calculated by laminar theory for both a hemisphere nose and a flat nose. This comparison has been made by presenting the ratio of the local heat-transfer coefficient to the stagnation-point heat-transfer coefficient for a hemisphere of the same diameter. The calculations were made by the laminar theory presented in reference 4 for both the hemisphere and flat noses. The experimental data for the hemisphere (ref. 5) and the flat noses were obtained in the preflight jet under sea-level conditions at M = 2.0. (The test results indicated transition at about $S/S_1 = 0.33$.) Comparison of these values with those for the concave nose shape at 0° angle of attack indicates that the local heat-transfer coefficients on the concave nose are lower than both theoretical and experimental values for either the flat or the hemisphere nose, until $S/S_1 = 0.825$ or S = 3.25 inches. The heat-transfer coefficient at the stagnation point is approximately 40 percent of that on the hemisphere.

Another comparison may be made on the basis of total heat input. In this case it is important to remember that the hemisphere and the concave nose have twice the surface area as that of the flat-face model. The following chart shows the comparison in total heat input for a Mach number of 2.0; however, reference 2 shows a different relationship in total heating for higher Mach numbers:

Nose shape	Data obtained by -	Total heat input, Btu/sec
Hemisphere	Laminar theory	374
Hemisphere	Experiment	957
Flat face	Experiment and laminar theory	255
Concave	Experiment	536

Comparison of the experimental heat-transfer distribution of a hemisphere where transition occurs at $S/S_1 = 0.33$ shows that the total heating is 1.8 times higher than experimental values for the concave nose. Since the freestream Reynolds numbers for the tests of the concave and the hemisphere noses were about the same, this comparison indicates that the concave nose might be extremely worthwhile in conditions where transition would be expected on a hemispherical nose.

The nose shape reported herein was investigated by the Langley Pilotless Aircraft Research Division on a two-stage rocket-propelled model at Mach numbers between 3 and 7. These unpublished data indicated stagnation-point values of only one-tenth to one-twentieth of those of the hemisphere. Other tests as discussed in reference 6 indicate two types of flow about the nose, steady and unsteady flow. Both types of flow were observed under the same flow conditions and no reason could be given to explain the two types of flow. The heat-transfer coefficients measured in reference 6 for the unsteady flow were approximately 6 to 7 times the coefficients for the steady flow. The steady-flow coefficients in the tests of reference 6 varied from 20 percent to 50 percent of the values at the stagnation point of a hemisphere. The differences between the apparently steady flow results of the present test, the tests of reference 6, and the flight tests have not been explained as yet.

CONCLUSIONS

From tests made in the preflight jet of the Langley Pilotless Aircraft Research Division (at its testing station at Wallops Island, Va.) at a Mach number of 2 and sea-level Reynolds numbers on a concave nose, the following results are evident:

1. Pressures measured up to 60° on the concave part of the model were equal to the total pressure behind the shock at angles of attack of 0°, ±5°, and ±10°. The lip of the model experienced free-stream static pressures at 0° angle of attack.

2. The heat-transfer coefficient at the stagnation point at 0° angle of attack is approximately 40 percent of that on the same size hemisphere.

3. The highest local heat-transfer coefficient was measured immediately inside the lip; this heating was of the same magnitude for all angles of attack. The heat-transfer coefficient on the lip at an angle of attack windward of 10° was lower than that experienced immediately inside the lip.

4. Comparing the concave nose and the hemisphere, which were tested at the same free-stream Reynolds number, on the basis of total heat input, the hemisphere was heating 1.8 times higher. This comparison indicates that the concave nose might be extremely worthwhile in conditions where transition would be expected on a hemispherical nose. However, other tests on concave noses indicate the possibility of unsteady flow conditions in the cup which give a large increase to the total heat input. At present, the conditions under which these unsteady flows are obtained are not understood.

Langley Aeronautical Laboratory,
National Advisory Committee for Aeronautics,
Langley Field, Va., February 27, 1958.

REFERENCES

1. Carter, Howard S., and Bressette, Walter E.: Heat Transfer and Pressure Distribution on Six Blunt Noses at a Mach Number of 2. NACA RM L57C18, 1957.

2. Hopko, Russell N., and Strass, H. Kurt: Some Experimental Heating Data on Convex and Concave Hemispherical Nose Shapes and Hemispherical Depressions on a 30° Blunted Nose Cone. NACA RM L58A17a, 1958.

3. Lucks, C. F., Bing, J. F., Matolich, J., Deem, H. W., and Thompson, H. B.: The Experimental Measurement of Thermal Conductivities, Specific Heats, and Densities of Metallic, Transparent, and Protective Materials - Part II. AF Tech. Rep. No. 6145 (Contract No. AF 33(038)-20558), Battelle Memorial Inst., July 1952.

4. Lees, Lester: Laminar Heat Transfer Over Blunt-Nosed Bodies at Hypersonic Flight Speeds. Jet Propulsion, vol. 26, no. 4, Apr. 1956, pp. 259-269.

5. Chauvin, Leo T., and Maloney, Joseph P.: Experimental Convective Heat Transfer to a 4-Inch and 6-Inch Hemisphere at Mach Numbers From 1.62 to 3.04. NACA RM L53L08a, 1954.

6. Cooper, Morton, Beckwith, Ivan E., Jones, Jim J., and Gallagher, James J.: Heat-Transfer Measurements on a Concave Hemispherical Nose Shape With Unsteady-Flow Effects at Mach Numbers of 1.98 and 4.95. NACA RM L58D25a, 1958.

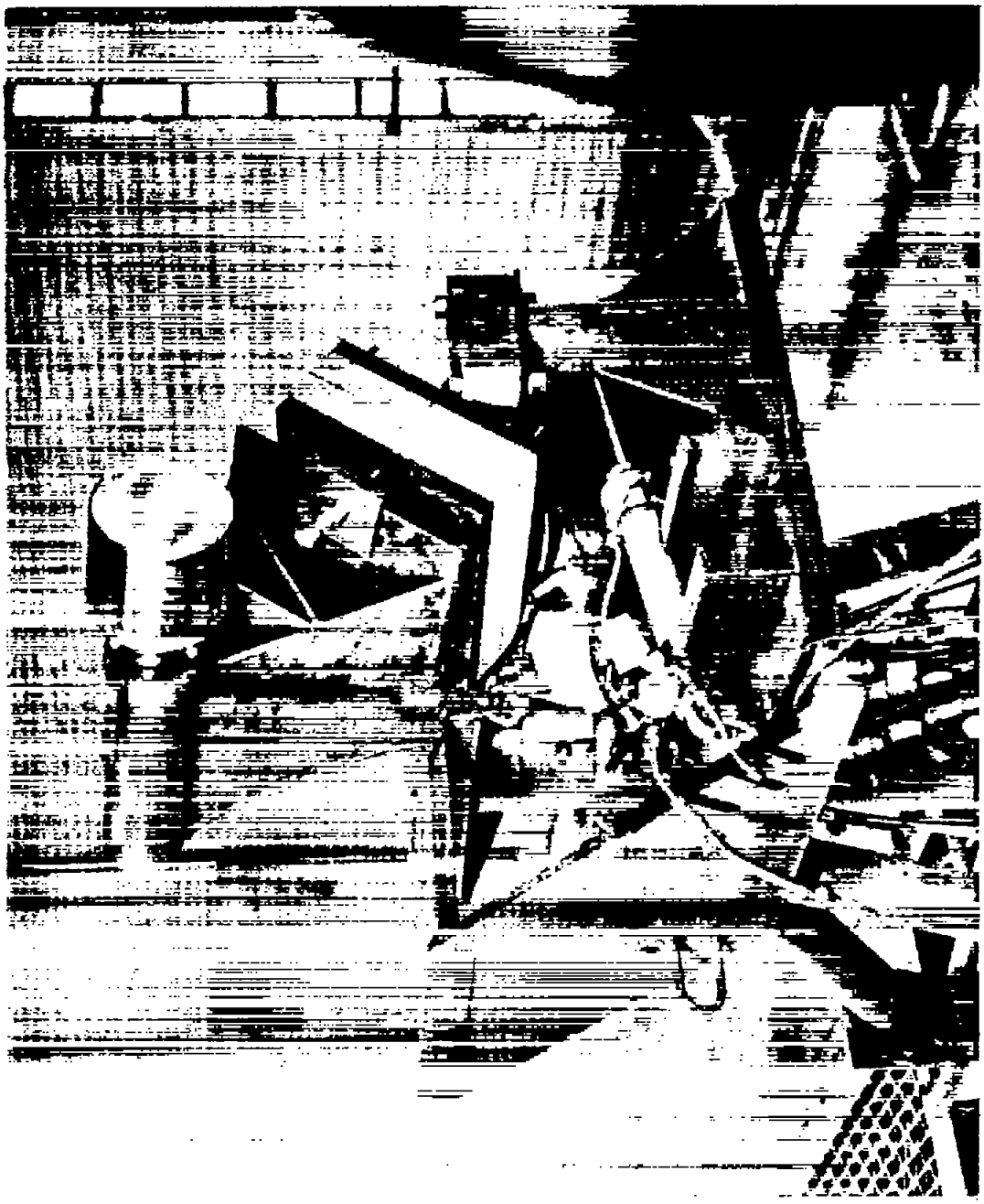

Figure 1.- Photograph of model before swinging into jet stream. L-57-3832

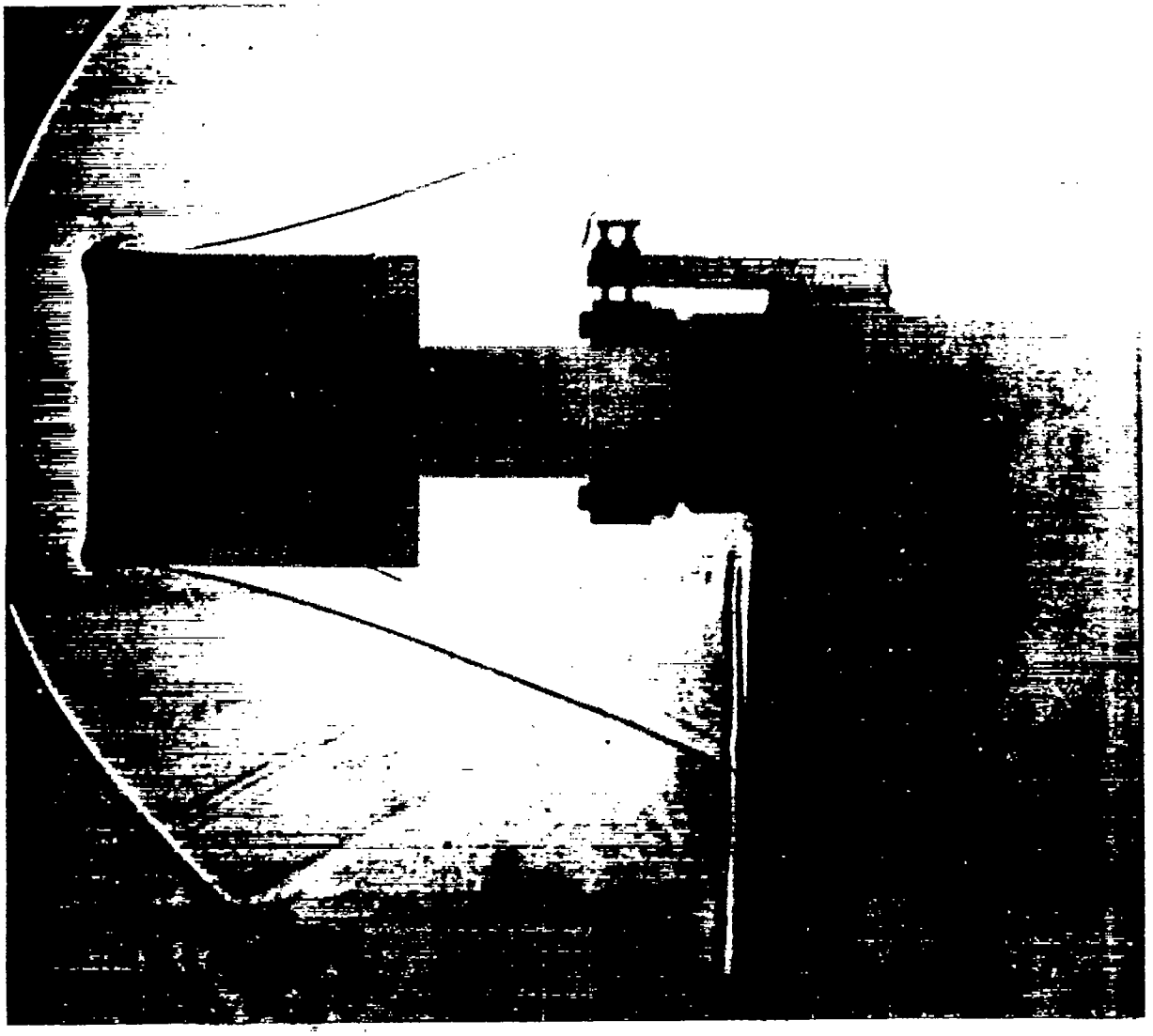

Figure 2.- Shadowgraph of model at angle of attack of 0°. L-58-1610

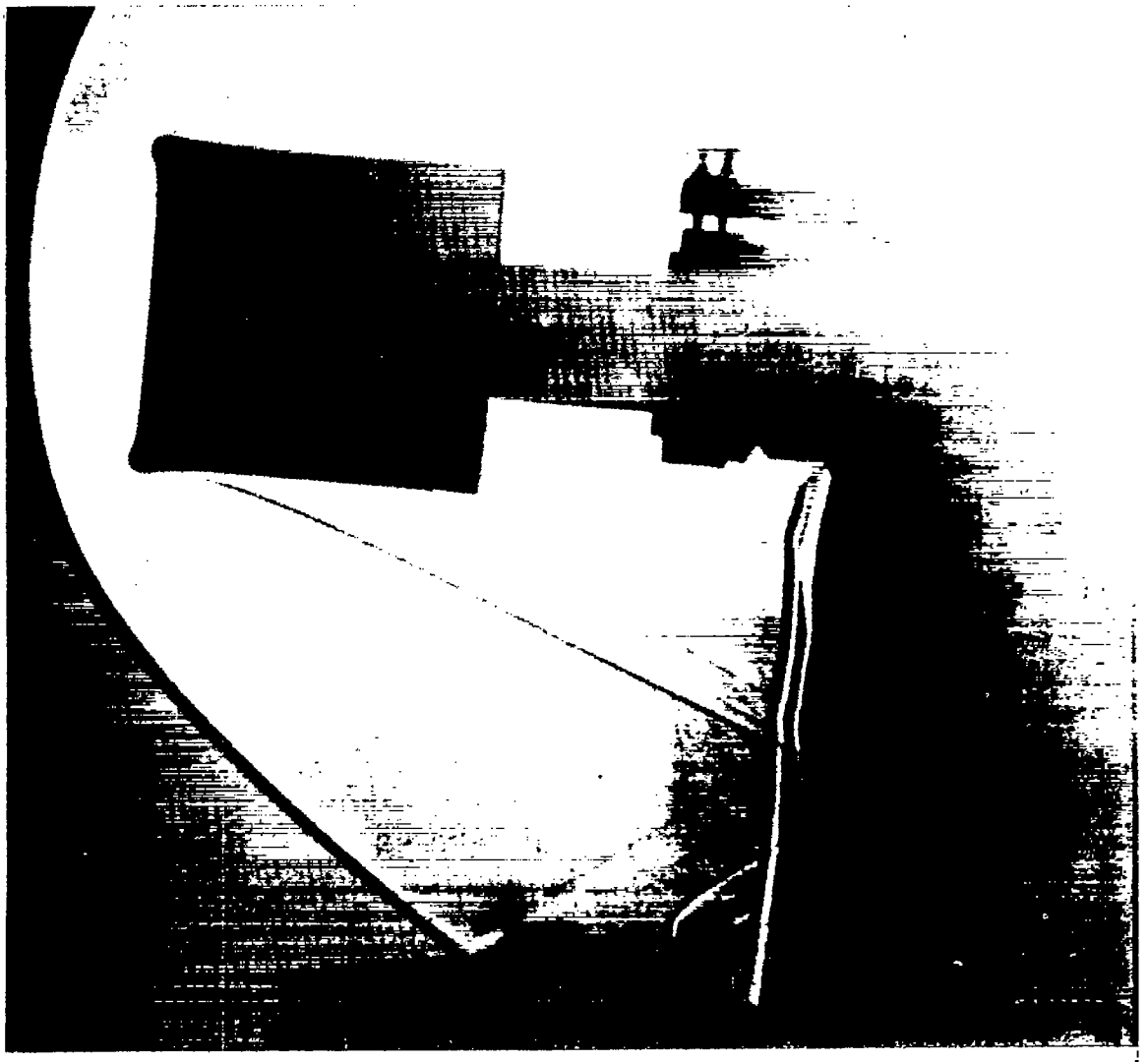

Figure 3.- Shadowgraph of model at angle of attack of 5°. L-58-1611

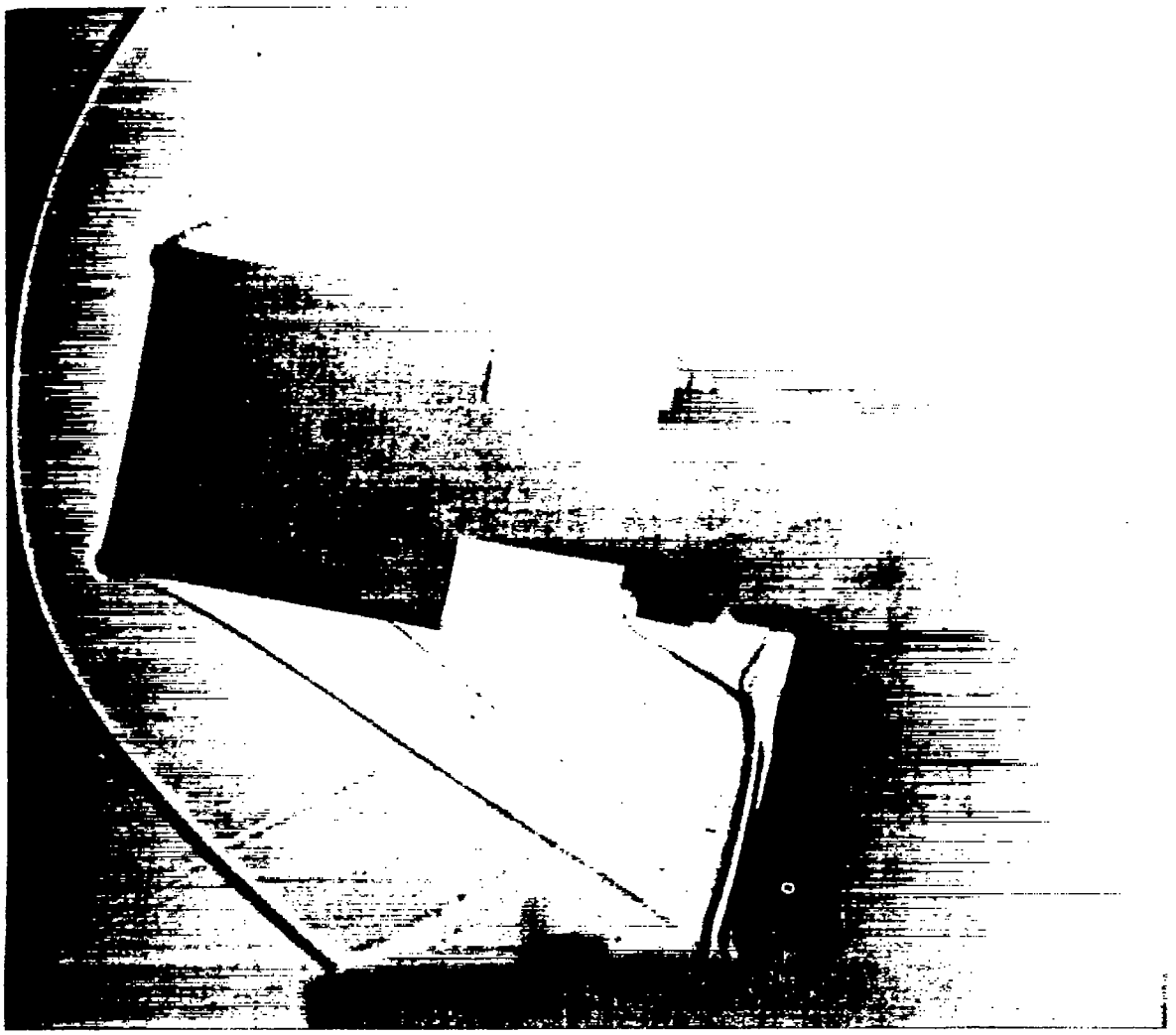

Figure 4.- Shadowgraph of model at angle of attack of 10°. L-58-1612

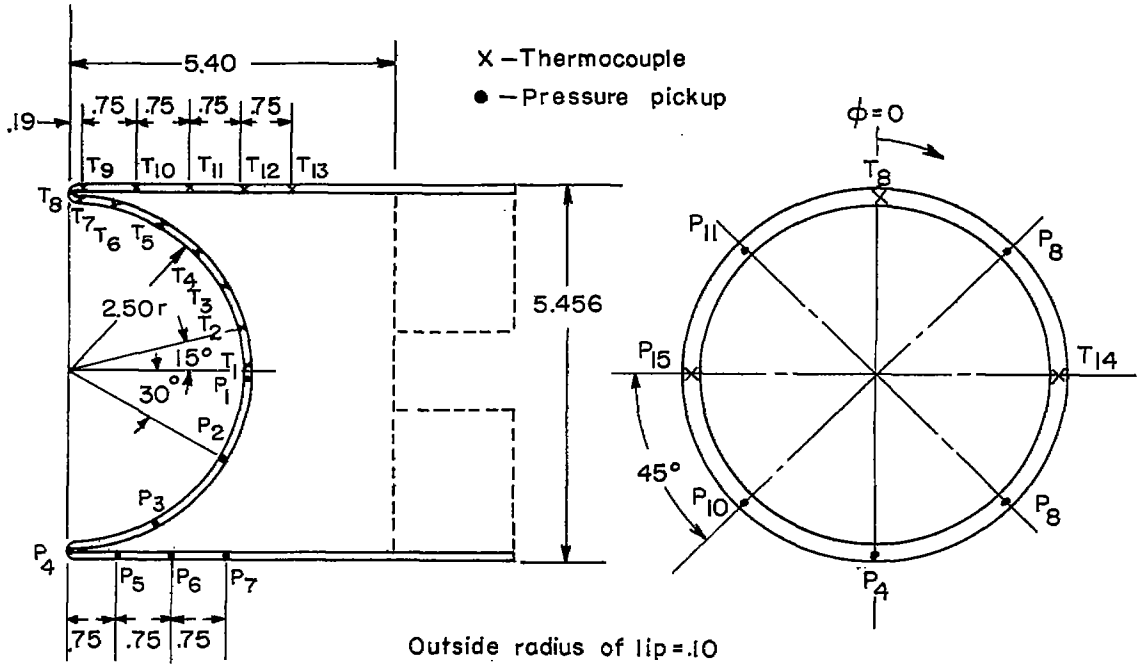

All measurements in inches

Thermocouple station (a)	Distance measured along surface from center line, S, in.	Skin thickness, t_w, in.	ϕ, deg	Pressure station (a)	Distance measured along surface from center line, S, in.	ϕ, deg
1	0	0.038	0°	1	0	0°
2	.66	.038	0	2	1.31	0
3	1.31	.039	0	3	2.62	0
4	1.96	.045	0	4	3.96	180
5	2.62	.043	0	5	4.73	0
6	3.27	.049	0	6	5.48	0
7	3.75	.053	0	7	6.23	0
8	3.96	.061	0	8	3.96	45
9	4.17	.050	0	9	3.96	135
10	4.92	.050	0	10	3.96	225
11	5.67	.053	0	11	3.96	315
12	6.42	.052	0			
13	7.17	.052	0			
14	3.96	.061	90			
15	3.96	.061	270			

[a]Thermocouple and pressure pickups are numbered in order from center line.

Figure 5.- Sketch of model and station locations.

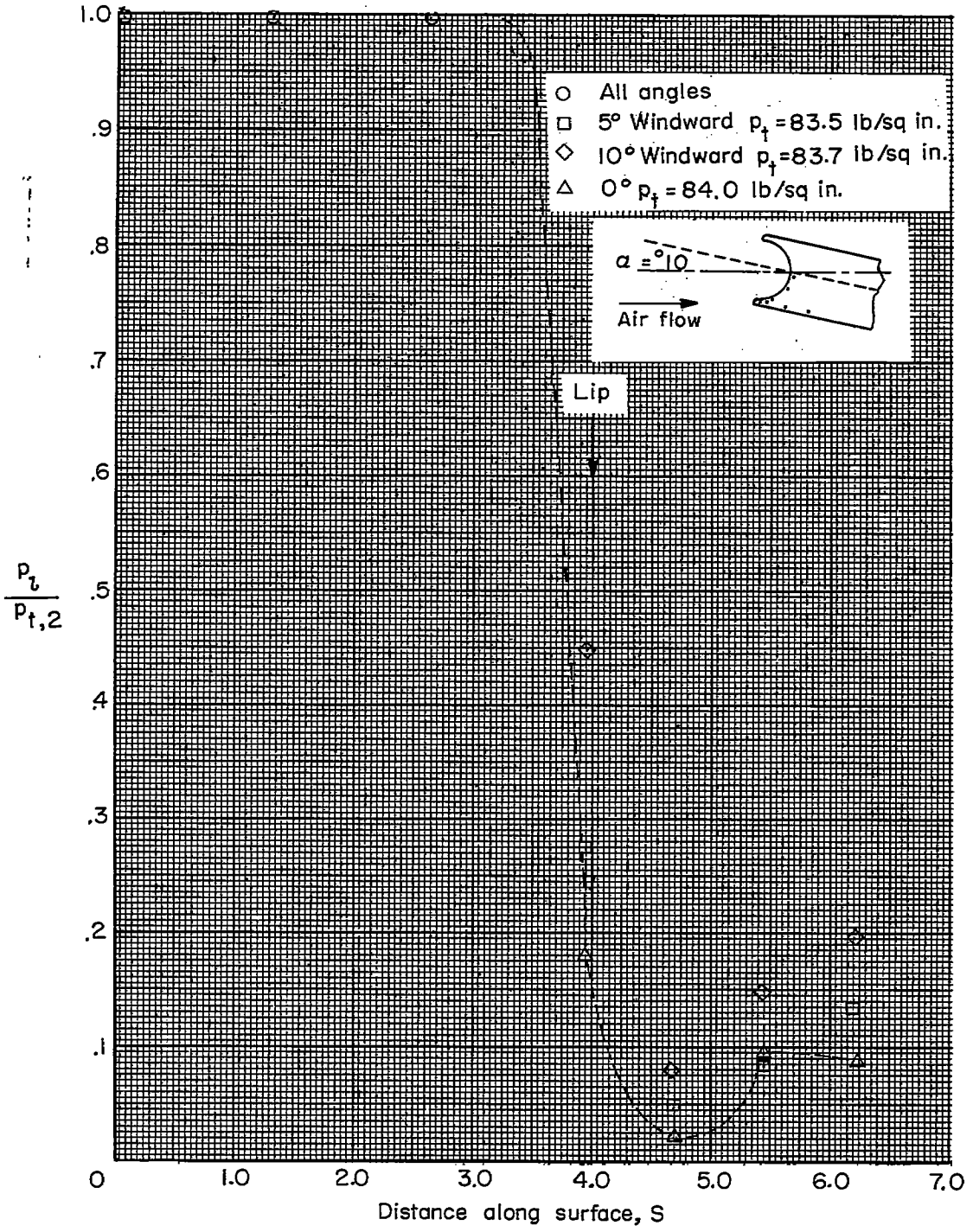

Figure 6.- Pressure distribution at windward angle of attack.

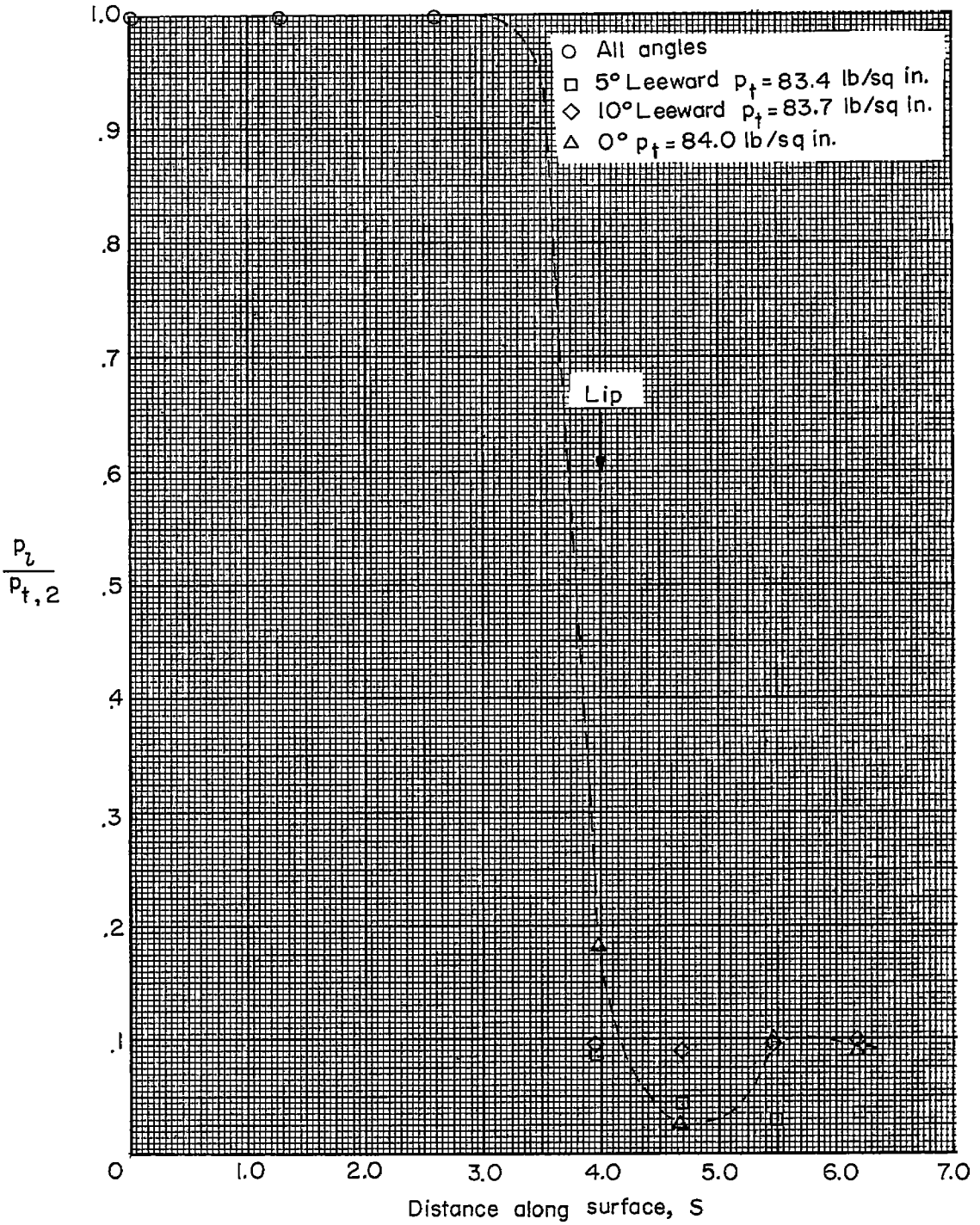

Figure 7.- Pressure distribution at leeward angle of attack.

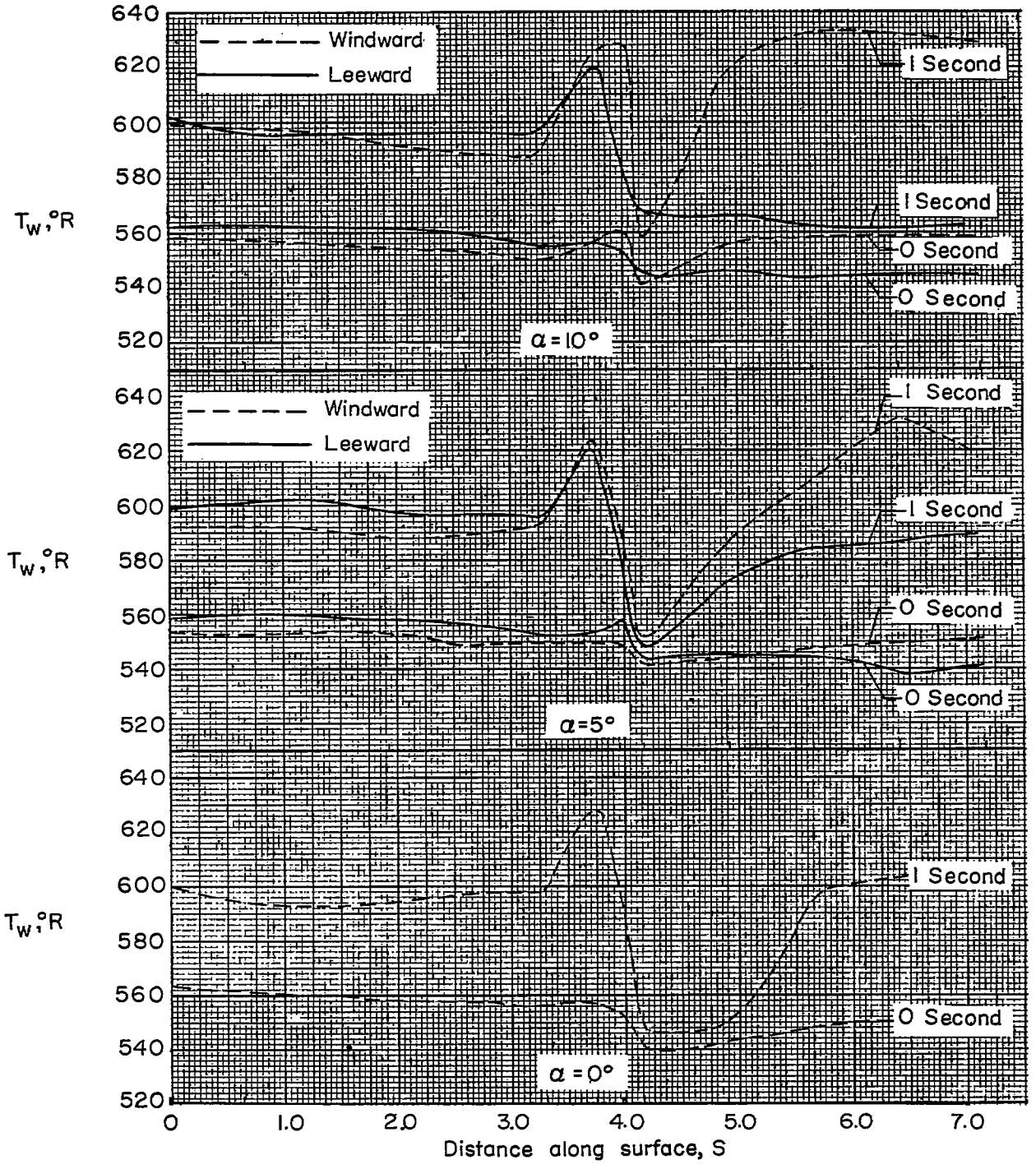

Figure 8.- Wall-temperature distribution for 0°, 5°, and 10°.

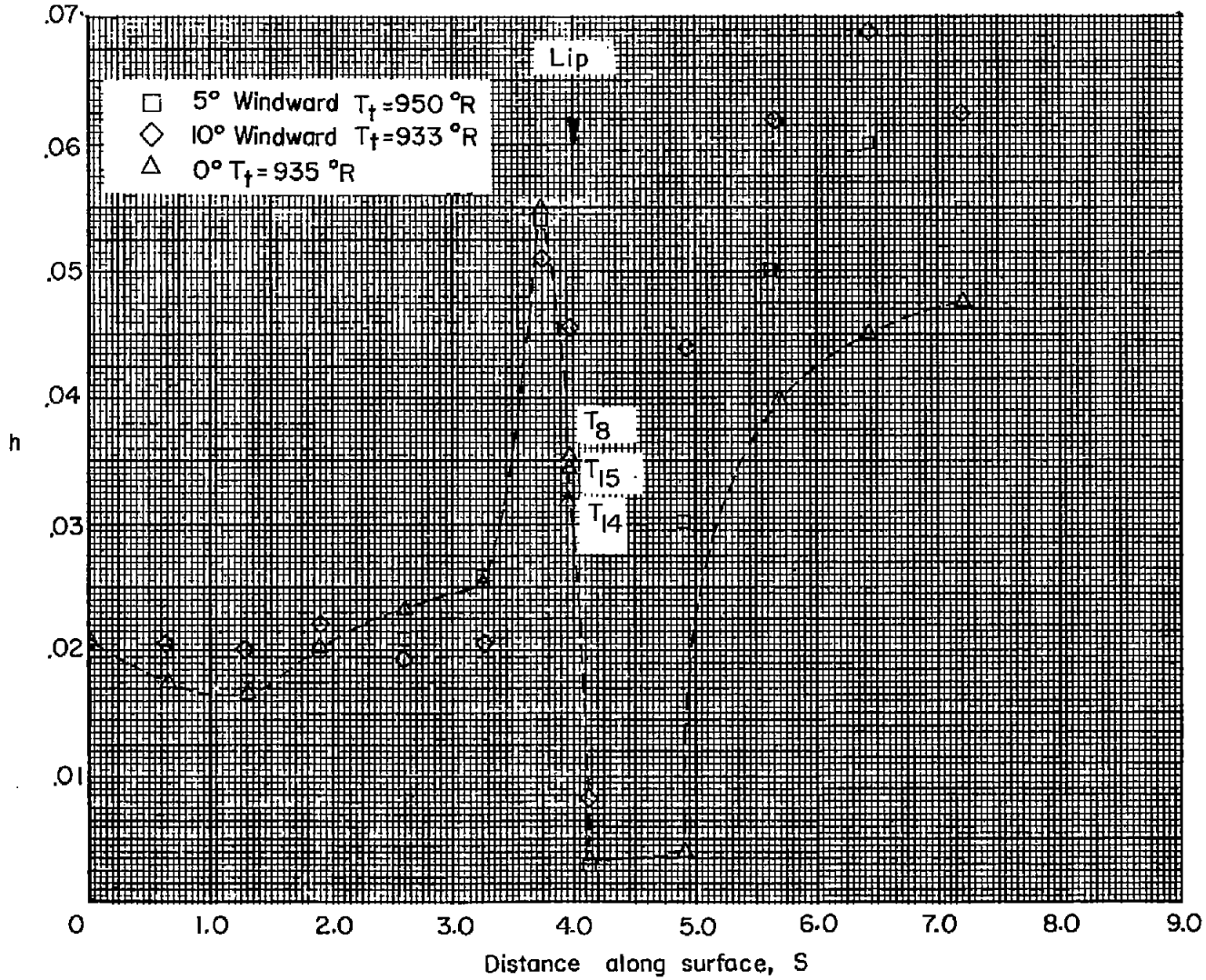

Figure 9.- Heat-transfer coefficients at windward angle of attack.

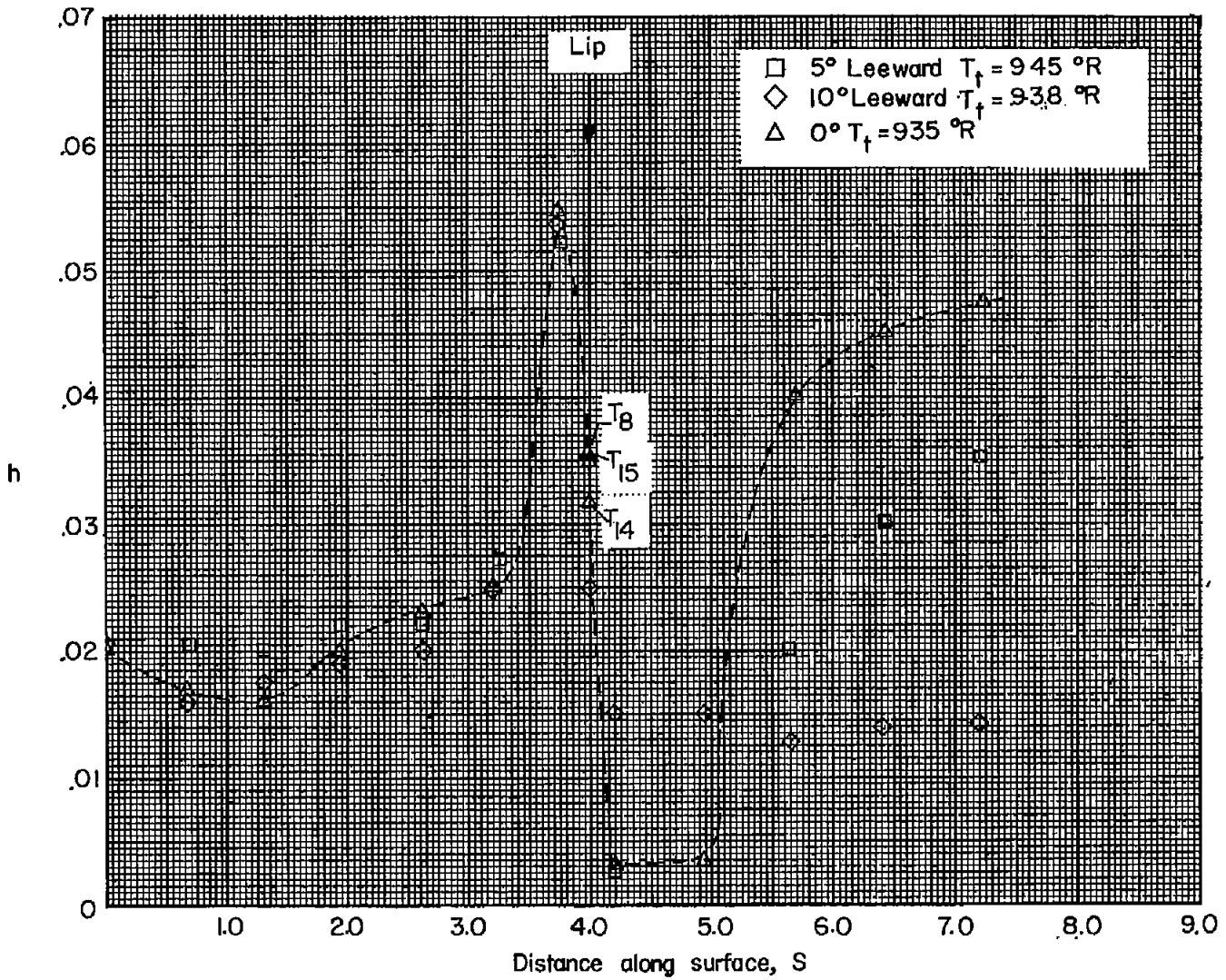

Figure 10.- Heat-transfer coefficients at leeward angle of attack.

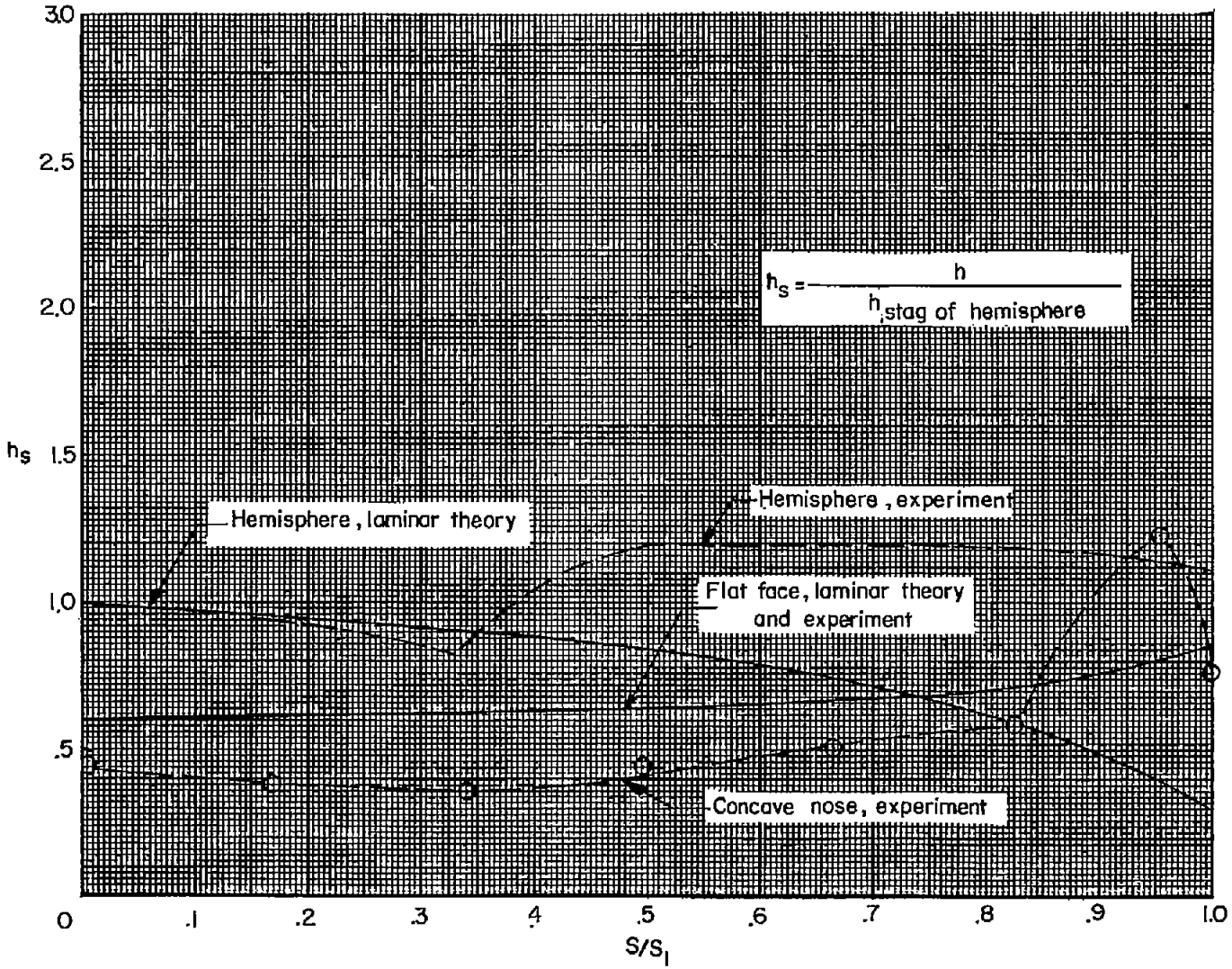

Figure 11.- Comparison of heating rates for hemisphere, flat-face, and concave noses.